Characterization of the Eugene Stansbery-Meter Class Autonomous Telescope on Ascension Island

Corbin L. Cruz[1]
corbin.l.cruz@nasa.gov
Brent A. Buckalew[1], **Susan M. Lederer**[2], **Kayley Green-Tooney**[3], **Paul Hickson**[4], **Timothy F. Kennedy**[2], **Heather M. Cowardin**[2]
[1]*Jacobs JETS contract, NASA Johnson Space Center*
[2] *NASA Johnson Space Center, Orbital Debris Program Office*
[3]*Texas State University*
[4]*University of British Columbia/Euclid Research*

ABSTRACT

In a focused effort to meet full operational capability for NASA's Eugene Stansbery-Meter Class Autonomous Telescope (ES-MCAT), a thorough system characterization analysis was completed. NASA's Orbital Debris Program Office (ODPO) utilizes ES-MCAT as the primary sensor for characterizing the geosynchronous Earth orbit (GEO) environment to acquire photometric data of small, faint debris objects in or near GEO. ES-MCAT is located on Ascension Island in the middle of the Atlantic Ocean at nearly 8° South latitude and 14° West longitude. This location provides dark skies suited for faint object observations but is also continuously subject to a harsh environment exposed to volcanic ash and salt spray. To better assess the overall system performance of the optical instrument, a historical assessment of the system's performance was conducted. This analysis investigated all systematic and optical operational data to determine the overall performance parameters for ES-MCAT.

A complete optical system throughput calculation was performed to determine the optimal filter for observing orbital debris in GEO orbits. The responses of each optical component to the solar spectrum, with atmospheric absorption, were multiplied and integrated to give ES-MCAT's total system response for various filters. With the highest flux values, the Sloan Digital Sky Survey (SDSS) r′ and g′ were determined to be the optimal filters for ES-MCAT observations. Further analysis with known GEO debris objects enabled the selection of the r′ filter for characterization of the GEO debris population. A detailed overview of the optical system throughput, data reduction, photometric and astrometric data, and other system characteristics that define ES-MCAT are discussed.

1. INTRODUCTION

The Eugene Stansbery-Meter Class Autonomous Telescope (ES-MCAT) is a 1.3-meter Ritchey-Chrétien telescope located on Ascension Island in the Atlantic Ocean. This telescope is capable of orbital debris observations with its current goal of completing a geosynchronous Earth orbit (GEO) survey of debris objects to support future Orbital Debris Engineering Model releases [1]. ES-MCAT currently operates autonomously with the aid of the Observatory Control Software (OCS), which both controls the observatory and processes data after nightly observations [2]. To understand the capabilities of the telescope and OCS, along with testing the system's capabilities for conducting a GEO survey, we completed several studies from observational data. These analyses and their outcomes are discussed in this paper.

We first characterize the complete optical throughput of the telescope and give an overview of the corresponding optical components, ultimately leading to the decision of which filter to use for the GEO survey. Next, a validation of the photometric and astrometric observational data results using OCS is presented. OCS's ability to compute values such as zeropoints, signal-to-noise ratios (SNRs), full width at half maximum (FWHM), and plate solution are then discussed. Lastly, the limiting magnitude and assessment of completeness of objects detected with the fully integrated ES-MCAT telescopic system (hardware and OCS) are presented.

2. OPTICAL SYSTEM THROUGHPUT

ES-MCAT's complete optical system is comprised of multiple optical components including the coated primary mirror, secondary mirror, field corrector, CCD, and filters. The primary mirror is coated with a protected, enhanced silver coating (by ZeCoat), which performs significantly better and is expected to be more durable than protected aluminum (the primary mirror's original coating) [3, 4]. The secondary mirror is coated with enhanced aluminum by L&L Optical Services [5]. An aspheric field corrector also lies within the optical path to flatten and correct astigmatism over the 0.96-degree (diagonal) un-vignetted field of view of ES-MCAT. A Spectral Instruments 1100S CCD is the prime camera used by ES-MCAT with an anti-reflection (AR) coated, fused silica window. Currently installed in ES-MCAT's camera and cooled to -110°C is a Grade 1 e2v BI deep-depleted, astro broadband-coated chip [6], which has a better quantum efficiency (QE) at the blue end than the red when compared to a previously installed CCD chip. Finally, a set of research grade Sloan Digital Sky Survey (SDSS) g′r′i′z′, and Johnson/Bessel-Cousins BVRI filters, manufactured by Custom Scientific with a robust sputtered coating, are installed in the 8-position filter slide [7]. The optical response of the mirrors' reflectance, field corrector's transmittance, CCD window's transmittance, and CCD QE over the visible and near infrared spectra (limited to the 350-1100 nm spectral range of the CCD) is presented in Fig. 1. The transmittance of all eight filters is shown for each filter set in Fig. 2. These values were provided by their manufacturers [4-8].

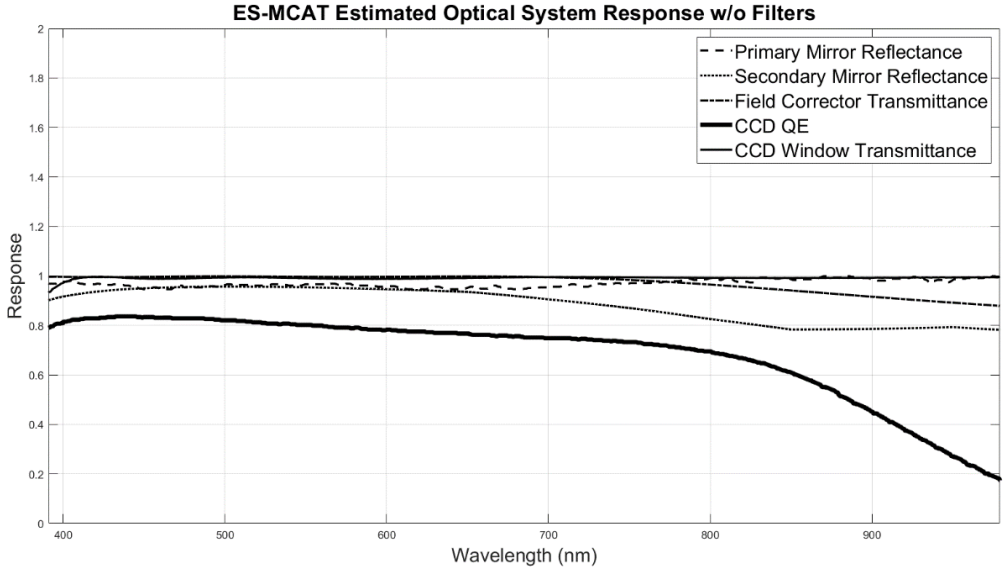

Fig. 1. Response of each optical component in the light path.

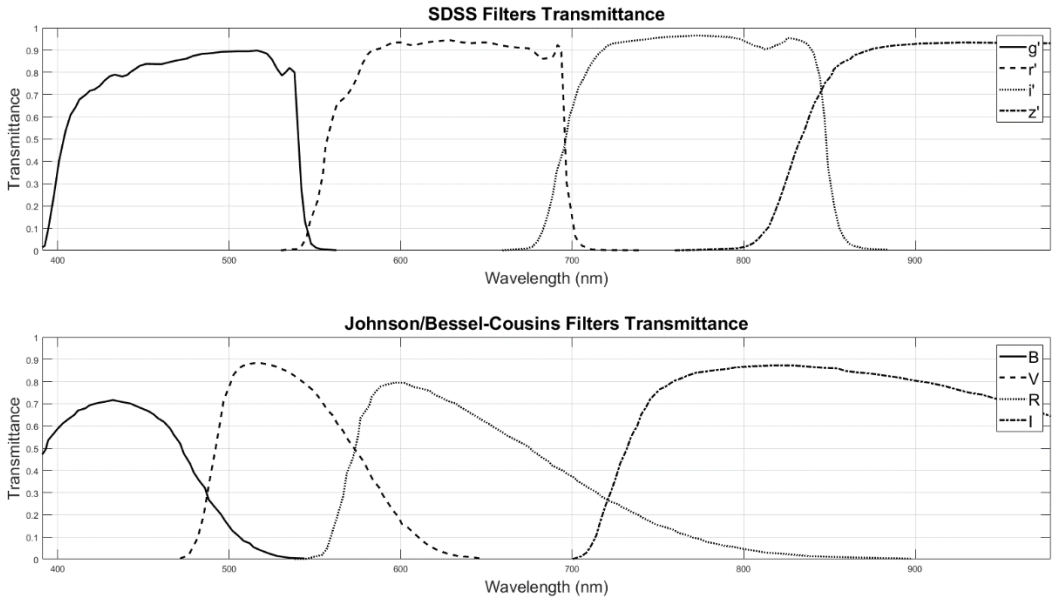

Fig. 2. Transmittance of the SDSS g′r′i′z′ and the Johnson/Bessel-Cousins BVRI filters. The filters labeled consecutively in the legends correspond to the filter curves from left to right.

The primary goal of ES-MCAT is characterizing the orbital debris environment in GEO, and solar illumination is the predominant source of reflected light from debris objects (Earthshine is neglected). To assess the full system throughput, the solar spectrum is used in this analysis as measured though atmosphere at sea-level. As with all spectral data, the response of the solar spectrum can vary, and thus an average was calculated [9 – 11]. Each spectrum was linearly interpolated separately between the wavelength regions of interest and were then averaged together to yield the result shown in Fig. 3.

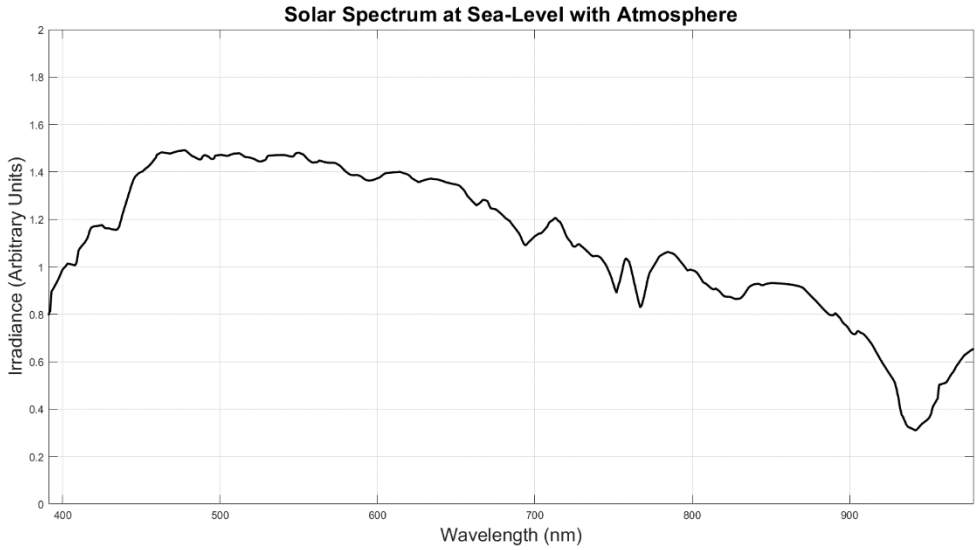

Fig. 3. The average solar spectrum in irradiance or flux units, from 350-1000 nm at sea level [9], [10], [11].

The response data of each component of ES-MCAT was linearly interpolated for the different optical filter band passes (SDSS and Johnson/Bessel-Cousins filters). The interpolated response data for all components were then

multiplied together so that the entire optical system would be represented for each filter. Next, the throughput from the optical components discussed above was combined with the expected typical transparency of the atmosphere at ES-MCAT's altitude/location for the g′r′i′z′ and BVRI filters. Finally, this result was integrated to give the total system response for each filter (bandpass) in arbitrary flux values. These results are sufficient, as only the comparative values between each filter are of interest. These flux values helped to inform which filter should be used to achieve the highest signal-to-noise ratio (SNR) on average for this specific optical system.

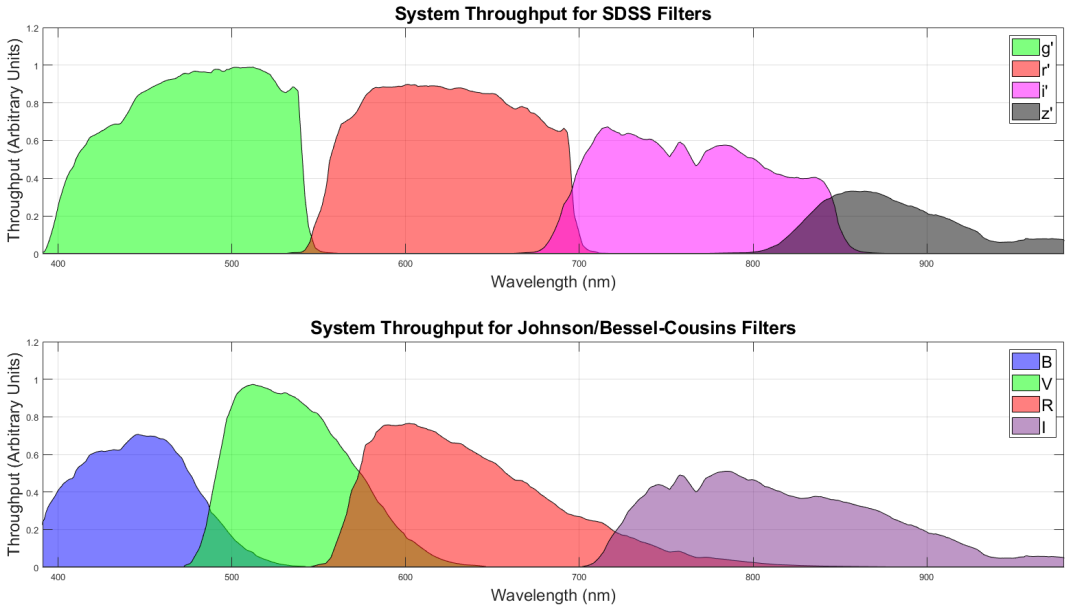

Fig. 4. Full system throughput is shown for each filter bandpass. This includes all optical components and the effects of the solar spectrum (the typical source of reflected light from debris objects).

Table 1: Relative throughput flux for each filter, with all optical components and atmospheric effects applied.

Filter	Flux (Arbitrary Units)
g′	118 ± 1.36
r′	116 ± 1.35
i′	82.8 ± 0.998
z′	30.9 ± 0.560
B	56.0 ± 1.04
V	81.6 ± 1.23
R	89.7 ± 1.22
I	75.5 ± 0.855

As shown in Fig. 4 and Table 1, the SDSS g′ and r′ filters have the highest relative flux value throughput and have overlapping uncertainties. The reflectivity of materials that compose debris varies greatly across the visible and near infrared bandpasses. To select between the two filters with the highest flux values, test data were taken with ES-MCAT of a variety of cataloged debris fragments at GEO. To enable comparison of ES-MCAT data with data from optical telescopes previously used by the NASA Orbital Debris Program Office (ODPO), which were centered on red bandpasses, these studies, like previous studies, supported r′ as the filter of choice for ES-MCAT when operating under nominal conditions of collecting data on GEO debris. The previous primary telescope used for the ODPO's optical measurement program, the Michigan Orbital Debris Survey Telescope (MODEST), utilized a broad R filter, centered at 630 nm- and 200 nm-wide FWHM, to maximize the signal throughput for GEO orbital debris detections.

3. OCS PHOTOMETRY AND ASTROMETRY VALIDATION

The data for the OCS photometric and astrometric validation were taken with ES-MCAT over four different observation nights in 2020, specifically 3 May, 9 June, 26 June, and 14 July. For each night, a 10-second SDSS r′ image of a stellar field was acquired (each stellar field typically has hundreds of stars). For the nights of 9 and 26 June 2020, two different stellar fields were chosen, resulting in a total of six observation/photometry files. After OCS processed each image, which included flat fielding, bias subtraction, and astrometric calibration, OCS generated photometry files of all point sources in the sidereal images.

A portion of these photometry files includes the FITS image header information; e.g., exposure time, date/time of observation, pointing of the telescope for that image (field center), airmass, which filter was used, and the cloud density at the start and end of the exposure. A FLIR infrared camera measures the cloud opacity while the observatory is open, and these measured values are approximately equal to the atmospheric extinction for values that are less than 4.0. A line of data for each detected object in the image is also included in the photometry file. Each detection includes the International Celestial Reference System (ICRF) right ascension (RA) and declination (Dec) coordinates, apparent magnitudes, zeropoints, etc.

An excerpt of a photometry file highlighting a detected object is shown in Fig. 5. The first row indicates the file's type. The second row includes the column headers for the various parameters from a single point source. The third row is an example of a point source's measurements. The object column includes the numbered objects within an observed night. X and Y are the approximate positions on the CCD where the units are pixels. RA and Dec are measured in the sexagesimal system. The apparent magnitude is the calibrated apparent magnitude of the object. A and B are the FWHM ellipse's major and minor axes of the point source and have the units of arcseconds. PA is the position angle of the FWHM ellipse starting from north and going east. SNR is the signal-to-noise ratio for this apparent magnitude. NPIX is the number of full pixels summed for this point source. RA_UNC, DEC_UNC, and MAG_UNC are the RA uncertainty, Dec uncertainty, and magnitude uncertainty, respectively. The units of astrometric uncertainties are degrees.

```
# OCS PHOTOMETRY FILE
# object      x        y          ra          dec       mag     a     b      pa     snr  npix   ra_unc   dec_unc  mag_unc
     47  121.2  3408.2  18:11:59.62  -05:37:29.8  12.21  4.04  3.86  135.00  505.8     2  0.00033  0.00011     0.19
```

Fig. 5. Example entry in an OCS photometry file for a detected object.

To characterize the accuracy of the OCS magnitudes, a comparison was made against GAIA Data Release 2 (DR2) magnitudes. The GAIA DR2 provides astrometry and photometry values for a multitude of stars with low uncertainties (on the order of a fraction of a milliarcsecond for astrometry and thousandths of a magnitude for photometry), making this data excellent for comparison. The RA and Dec values from at least 100 random point sources in each of the 6 photometry files were extracted. Then these files were used with the VizieR catalog website to correlate GAIA DR2 point source measurements with those point source measurements from OCS in terms of both brightness and position [12]. The SDSS r′ magnitudes were calculated from the GAIA DR2 data using the following formula:

$$r' = Gmag + 0.12879 - 0.24662 \cdot (BP - RP) + 0.027464 \cdot (BP - RP)^2 + 0.049465 \cdot (BP - RP)^3,$$

where r′ is the SDSS r′ magnitude, Gmag is the GAIA DR2 output, and BP-RP is the GAIA DR2 color output. This formula was taken from section 5.3.7 from the Gaia DR2 manual [13].

With the OCS SDSS r′ magnitude and the GAIA derived SDSS r′ magnitude, it is possible to determine how accurate OCS's magnitudes are when compared to the GAIA measurements. First, the differences between the two SDSS r′ magnitudes are calculated from the four nights of six total images. The range of absolute differences is calculated for the four nights and is presented in Table 2.

Table 2: Range of SDSS r′ magnitude differences between those from OCS and GAIA DR2.

Night	Min SDSS r′ Difference	Max SDSS r′ Difference
3 May 2020	0.000563	1.254
9 June 2020	0.001023	7.49
26 June 2020	5.50E-05	1.5611
14 July 2020	0.001866	2.632

Some of these magnitude differences can be rather large. However, these differences could be statistically acceptable if the GAIA DR2 magnitude is within 3σ of the OCS magnitude in the photometry files. The following magnitude metric was generated to determine how many OCS magnitudes fall too far away from the 'true' GAIA DR2 magnitudes:

$$\text{Magnitude Metric} = |r'_{OCS} - r'_{GAIA}| - 3 \cdot \sigma_{mag\_unc},$$

where r'_{OCS} is the OCS generated r′ magnitude, r'_{GAIA} is the GAIA DR2 derived SDSS r′ magnitude, and σ_{mag_unc} is the uncertainty of the OCS magnitude. The total number of point sources with differences between OCS and GAIA magnitudes that are more than 3σ from the 'true' magnitudes is shown in Table 3.

Table 3: Number of point sources with differences between OCS and GAIA DR2 magnitudes greater than 3σ, with their possible explanations.

3	Overexposed Star
1	RR Lyrae star
9	Possible False Positive
9	Unknown Origin (2/9 ="Extragalactic")
22	TOTAL

For the 6 images and 764 point sources analyzed in these images, 22 point sources have differences in the OCS and GAIA magnitudes that cannot be explained by the uncertainties. Three of these problem sources are overexposed stars. One is a known RR Lyrae star. Nine are what OCS considers sources, but to the human eye no point source can be seen – which are indicated in Table 3 as possible false positives. Finally, the last nine are point sources of unknown origin with two of these unknowns looking extragalactic (i.e., other galaxies). For those seven unknown point sources that don't look extragalactic, these detections point out the difficulty of being able to ascertain every variable point source in the night sky. Thus, the simplest explanation for these seven failures is that they are variable stars that are currently not known. Further study of these point sources may reveal their nature. OCS mitigates the presence of unknown variable and extragalactic sources by using the median when deriving the zero point. At the worst, in terms of OCS's photometric accuracy, it is assumed that these seven are simply bad calibrations. In this case, the failure rate of OCS's photometry would be 0.9%, or a success rate of 99.1%. This success rate is off from the Gaussian distribution assumption of 99.8% which could mean that the stellar photometry is non-Gaussian, that the uncertainties do not account for all uncertainties in the system (examined in the next section), or that some of the seven unknown sources are variable and, therefore, should not be considered failures. Variable stars are quite common and are the likely culprit.

Similar to the previous results, it is possible to determine how effective OCS is at producing astrometric positions close to the results derived from GAIA DR2. First, the differences between the two astrometric positions are generated from the four nights of six images. The range of absolute differences is calculated for the four nights and is presented in Table 4.

Table 4: Range of astrometric differences between the RAs and Decs from OCS and GAIA DR2.

Night	Min Astrometric Difference (")	Max Astrometric Difference (")
3 May 2020	0.0768	2.12
9 June 2020	0.021	3.67
26 June 2020	0.0315	4.9
14 July 2020	0.0467	5.95

Some of these astrometric differences are as large as 10 pixels (~6"). However, these differences could be statistically acceptable if the GAIA DR2 astrometric positions are within 3σ of the OCS astrometric positions in the photometry files. The following astrometric metric is used to determine how many OCS astrometric positions are more than 3σ from the 'true' GAIA DR2 magnitudes.

$$\text{Astrometric Metric} = \sqrt{(\text{RA}_{\text{OCS}} - \text{RA}_{\text{Gaia}})^2 + (\text{Dec}_{\text{OCS}} - \text{Dec}_{\text{Gaia}})^2} - 3 \cdot \sqrt{\sigma_{\text{RA}}^2 + \sigma_{\text{Dec}}^2},$$

where RA_{OCS} is the OCS generated RA, RA_{Gaia} is the GAIA DR2 derived Right Ascension, Dec_{OCS} is the OCS generated Dec, Dec_{Gaia} is the GAIA DR2 derived Dec, σ_{RA} is the uncertainty of the OCS RA, and σ_{Dec} is the uncertainty of the OCS Dec. For the 6 images and 764 point sources analyzed in these images, 8 point sources have differences in the OCS and GAIA astrometric positions that cannot be explained by the uncertainties. Two of these problem sources are overexposed stars. One is a known high proper motion star. Finally, the last five are measurements where no point source can be seen by the human eye. Of those five unseen, three also failed the previous photometry validation analysis. It is assumed that those three are true indications that nothing was there. Technically, if the uncertainties were Gaussian in distribution and for the number of point sources analyzed, on average, one astrometric metric result should have been negative with no known explanation. It is assumed here that those two unseen point source measurements that just failed the astrometric metric were point sources. OCS will then have a failure rate of 0.26% or success rate of 99.74%. That success rate is almost the same as the theoretical Gaussian value of 99.8%. Therefore, it was determined that based on the data, there is no reason to suspect the accuracy of the OCS astrometric measurements given the uncertainties derived for the ES-MCAT optical system.

4. ZEROPOINT, SNR, FWHM, AND PLATE SOLUTION

While the overall in-frame photometric and astrometric calibration was tested and appears to do well according to the results in the previous sections, the individual components of the calibration need their own testing. Here, the OCS methods for determining the zeropoint, SNR, and FWHM are compared to those developed in the Image Reduction and Analysis Facility (IRAF), which is software that was developed by astronomers specifically for analyzing astronomical data. The plate solution is compared with results produced from the astrometric calibration service found within astrometry.net. The data used for the calculation of zeropoint, SNR, and FWHM are from images acquired on 14 July 2020, a subset of those used in the previous sections. However, the data for analyzing the plate solution were six images taken on 18 May 2020 and another six images taken on 9 June 2020.

IRAF commands were used on the OCS processed image to find the point sources in the images and then to perform aperture photometry of those point sources. From these commands, the *xy* pixel coordinates, magnitude, uncertainty, FWHM, and SNR of each point source were extracted. The zeropoint based on the IRAF results is calculated in the following manner. First, differences between the IRAF magnitudes and GAIA magnitudes are generated. Second, the median of those differences is found for the subsample of GAIA magnitudes between 9 and 16, which encompasses those point sources that are neither overexposed nor underexposed. These results were then compared to those from OCS like what was described in the previous sections.

The zeropoint generated from the IRAF results is 23.37±0.39 while OCS calculated a zeropoint of 24.05±0.12 for the same image. The medians of these values agree with each other to within 3σ. The discrepancy in the results is mostly attributable to the fact that the IRAF method uses aperture photometry and OCS uses something akin to a summation of Point Spread Function (PSF) fitting [2]. The OCS method is superior when dealing with crowded

fields like the numerous star trails in the GEO survey images. Also, it is possible to produce an IRAF magnitude metric similar to what was done in the previous section on OCS in-frame photometric calibration. Using the same sample of data (with hundreds of points sources analyzed), the IRAF magnitude metric fails for 8 point sources within all images, while OCS magnitudes failed for 12 point sources in all images. Both methods fail on the three overexposed stars, the one known RR Lyrae star, and four unknown stars (possible variable or extragalactic). OCS has problems with four other unknown sources. The reason that the IRAF method does not have problems with these other four images is because the uncertainties of the IRAF method are three times more than those for OCS (0.39 vs. 0.12 mag on average). With only a 33% reduction in failed metrics but with a 300% increase in the magnitude uncertainty, the IRAF aperture method is inferior to OCS's method given the necessary uncertainty increase.

The SNR results for these two methods (IRAF and OCS) should be one-to-one in a linear regression. The OCS results were placed along the Y axis, and IRAF results were placed along the X axis. The resulting regression has an adjusted R-squared value of 0.956, indicating that the linear regression explains 95.6% of the variation in the data representation. The slope of the linear regression is 1.057±0.006. While it is different from the theoretical 1.0, a slope of 1.057 has a percentage error of 5.7%. This difference from theoretical suggests that the OCS SNR values are elevated compared to those generated with the IRAF method. Thus, an OCS SNR of 6 is an IRAF SNR of 5.68. While observing fainter point sources in the GEO survey, OCS may spend more time working on matching these sources. However, so far there has not been a situation where the processing conducted by OCS for a full night's data has exceeded more than a day.

The median FWHM from the IRAF results is 2.72±0.59 while OCS's median FWHM is 3.20±0.47. Thus, both methods' median values agree with their values to within 3σ. Looking at individual methods, IRAF and OCS differ in their interpretation. For example, OCS is particularly good at measuring elongated FWHMs in one axis, which is caused by the apparent motion of the object across the CCD. This capability may be useful for orbital debris since some objects with large Dec rates will pass through the fields, and it is of interest for them to be detectable by OCS. However, this ability also brings a drawback. When two point sources are located close together, IRAF and the human eye can separate them and make an FWHM measurement of both sections, but OCS treats them as one object. This analysis was conducted on a stellar field and not a GEO survey image. In GEO survey images, two pieces of debris with similar brightness are not expected to be adjacent.

Calculating astrometric differences between the RA and Dec positions from OCS and astrometry.net, the median difference was 2.46E-4° (0.884"). Thus, the OCS method provides similar astrometric positions compared to other methods. OCS's average astrometric difference from the Gaia DR2 results is 4.78E-4° (1.72"). Astrometry.net's average astrometric difference from the Gaia DR2 results is 1.78E-3° (6.41"). Thus, OCS does a better job recreating astrometric results that are closer to the lower uncertainty results of the GAIA DR2 result. Also derived from both methods is a pixel scale of 0.61"/pixel which agrees with the theoretical calculations.

5. LIMITING MAGNITUDE AND COMPLETENESS

The limiting magnitude of an optical system reveals the faintest object that is detectable for a given set of observing criteria, and completeness indicates how well a system (e.g., telescope) can detect a point source of a specific magnitude. This section describes the estimation of the limiting magnitude that can be achieved by ES-MCAT's GEO survey along with the characterization of OCS's ability to detect objects of varying magnitudes. While the limiting magnitude was estimated from stellar sources using the sidereal tracking (ST) mode, the completeness study was performed with artificial point sources in rate track (RT) mode with the tracking rates in RA and Dec set to zero (the mode in which the GEO survey will be completed). In both cases, 10 second exposures, a minimum detection SNR of 6, and the SDSS r′ filter were used. In estimating the limiting magnitude, data from 53 nights between the dates of 16 April 2020 to 10 August 2020 were included. Data used in the completeness analysis include images taken on 12 June 2020.

The limiting magnitude estimation began by using a program independent from OCS to extract the date and time, image frame number, filter, exposure duration, FLIR value, and zeropoint for each ST image. Next, the program

parsed through each photometry file and selected the faintest apparent stellar magnitude. An excerpt of these parameters is included in Table 5 below.

Table 5: Parameters excerpt from limiting magnitude analysis.

Day of Year	Frame	Filter	Exposure (sec)	FLIR	Zero Pt	Dim Mag
189.3427	72	r'	10	0.05	24.41	19.15
189.3432	73	r'	10	0.08	24.36	19.23
189.3436	74	r'	10	0.04	24.37	19.23
189.3441	75	r'	10	0.01	24.37	19.24
189.3445	76	r'	10	0.01	24.38	19.27
189.3453	77	r'	10	0.03	24.38	19.24
189.3458	78	r'	10	0.04	24.43	19.25
189.3462	79	r'	10	0.03	24.40	19.24
189.3466	80	r'	10	0.03	24.40	19.24
189.3471	81	r'	10	0.00	24.41	19.24
189.3476	82	r'	10	0.00	24.39	19.26

To determine the limiting magnitude of ES-MCAT, the faintest detected magnitude in each image was plotted versus the FLIR extinction, seen in Fig. 6. The faintest magnitudes that were detected decrease as the FLIR values increase. This means that when there is more cloud cover, OCS can only detect brighter stars because the fainter stars are hidden by thin clouds. Both cloud variability and atmospheric turbulence contribute to the scatter in Fig. 6.

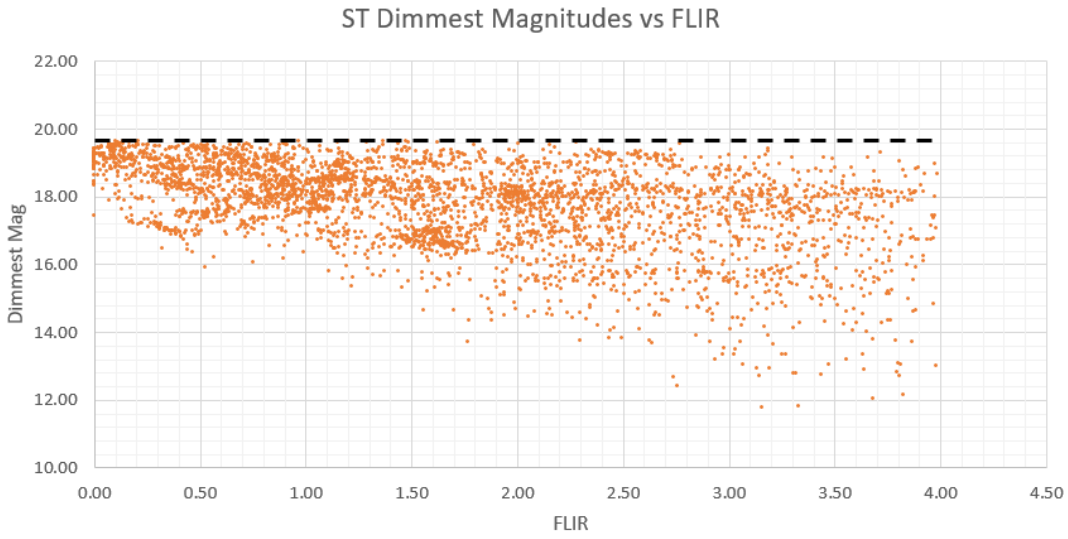

Fig. 6. ST images indicate the faintest magnitudes detected in each image versus FLIR extinction.

There also appears to be a clear, faintest (upper limit) magnitude regardless of the FLIR value. For further investigation into this trend, the faintest magnitude data points were separated into sections where the FLIR values were incremented by 0.25. The faintest magnitude value was then computed for each set, which were then averaged together. This averaged value, along with its standard deviation, produces a limiting magnitude. Based on the recent ES-MCAT configuration (April 2020 – August 2020), condition of optical components, operations, and data processing, the limiting magnitude to 1σ is 19.48 ± 0.18.

Having considered limiting magnitude, OCS's completeness values are detailed over the magnitudes detected by ES-MCAT for a GEO survey. For this study, completeness refers to how well the system (optical components and software) can detect objects at different magnitudes. During GEO observations in RT mode, observations are taken in sets of four to seven images. From a single night of observations, images were randomly chosen for the creation of artificial stars with the use of IRAF. A single point source was placed in each image with the same magnitude and pixel position for each set of 4 to 7 images, for a total of 120 images. For the results detailed below, the analysis and OCS processing of point sources was performed 5 times for the 120 images with magnitudes ranging from -10.5 to -8.5 in increments of 0.5. After the insertion of these artificial point sources, the modified images were processed with OCS, which then produced files that indicated whether a possible GEO object was observed. The magnitudes of the point sources that were found in these object detect files were placed in a detected results group. Since the object detect file only includes image sets where a point source is detected in at least four of the images in the image set, some positive detections may have been missed. If the artificial point source was found, the magnitude was recorded into the detected result group, and if the artificial point source was not found, it was placed in the undetected result group.

For those artificial point sources that were not detected by OCS, raw instrumental magnitudes were found. These instrumental magnitudes were then converted to calibrated SDSS apparent magnitudes and recorded. This process was then repeated for each apparent magnitude bin (incremented by 0.5).

Table 6: Relative Completeness of OCS ability to detect point sources in these magnitude ranges. Bins are labeled with their range.

Magnitude Bin	Detected	Not Detected
< 15.5	97%	3%
15.5-16	100%	0%
16-16.5	85%	15%
16.5-17	83%	17%
17-17.5	79%	21%
17.5-18	72%	28%
18-18.5	45%	55%
> 18.5	22%	78%

The positive and negative group results were binned using the Scott (1979) binning algorithm [14]. The right-most and left-most bins are summed with several bins to achieve a sample size for the bin of at least 40. This way, small number statistics could be avoided in their interpretation. The completeness results are presented in relative percentages for the various bins in both table (Table 6) and graphical form (Fig. 7). Note that there are uncertainties in these completeness percentages due to multiple factors including the binning method, OCS's processing uncertainties, and variations in the images themselves. Ultimately, the limiting magnitude of the system, ~19.5, dictates where the detection threshold goes to 0%.

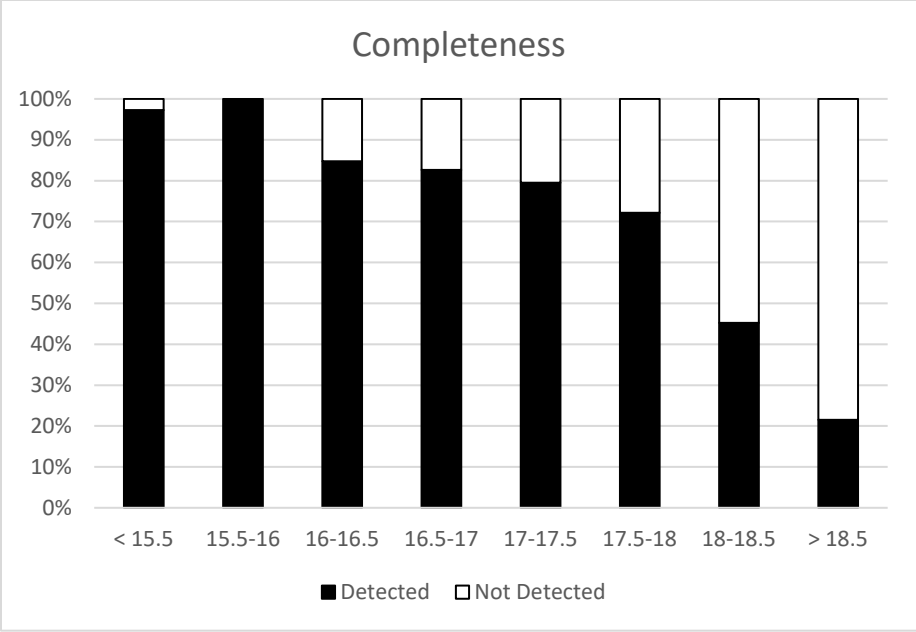

Fig. 7. Relative completeness of detections as a function of magnitude. Bins are labeled with their range. Black is the percentage of point sources detected by OCS. White is the percentage of point sources not detected by OCS.

6. SUMMARY

The complete optical characterization of ES-MCAT's optical system and components has been presented. The full throughput calculated the theoretical response of ES-MCAT's complete optical system from a given light source with the use of different bandpass filters. With the calculation of this system throughput and other considerations previously mentioned, a decision was made to conduct the GEO survey with the SDSS r′ filter for nominal conditions of collecting data on GEO debris.

For the system's overall photometric and astrometric performance, ES-MCAT and OCS work well in producing results that are suitable for a survey of debris in geosynchronous orbit. OCS works as well as other widely used image processing software such as IRAF. OCS along with ES-MCAT also produces similar astrometric plate solutions to other methods. OCS is an improvement in its astrometric reproduction of GAIA DR2 coordinates relative to IRAF. The astrometric solution generated by OCS performs well in deriving the correct RAs and Decs for the images from ES-MCAT. The uncertainties in RA and Dec are robust enough to explain the deviation of the astrometric positions generated by OCS from those astrometric positions from GAIA DR2.

The methodology that OCS uses to derive the zeropoint is sound and produces results comparable to other methods. OCS's system works well in crowded stellar fields, and the PSF fit ensures the background is not contaminated by faint sources (unlike the IRAF aperture photometry approach). The OCS method produces SNR values comparable to those from IRAF to within a 5.7% error. The OCS method produces comparable FWHM measurements to other methods to within their 3σ uncertainties. A bonus to the OCS measurement of FWHM is that OCS excels at measuring elongated objects like debris trails due to their large Dec rates.

Based on the recent ES-MCAT configuration, condition of optical components, operations, and data processing, the limiting magnitude for stellar sources in ST mode to 1σ is 19.48 ± 0.18. For comparison, MODEST, a 0.6-m telescope high in the mountains of Chile (vs. the sea level 1.3-m ES-MCAT) reached a limiting magnitude of 18.0 using the broad-R filter, 5-sec exposures, and an SNR of 10 [15]. While not an exact match of parameters, the higher SNR required and lower exposure time will somewhat balance the wider filter used by MODEST for an approximate comparison. Finally, OCS's ability to detect objects in RT mode (used for the GEO survey) with various magnitude values was characterized with respect to completeness.

The ODPO will continue using ES-MCAT for data collection focused on the GEO Survey to support future Orbital Debris Engineering Model releases. The data presented here is crucial to assess uncertainties in the optical data collected and to provide accurate uncertainties for orbital debris environmental data.

7. REFERENCES

[1] Lederer, S.M. *et al*., NASA's Orbital Debris Optical Program: ES-MCAT Nearing Full Operational Capability (FOC), *AMOS Technical Conference Proceedings, 2020*.

[2] Hickson, P. OCS: A Flexible Observatory Control System for Robotic Telescopes with Application to Detection and Characterization of Orbital Debris, *First International Orbital Debris Conference, Sugarland, Texas*, 2019.

[3] Wolfe, Jesse D. and Norman L. Thomas. "Durable silver coating for mirrors." U.S. Patent No. 6,078, p. 425, 20 Jun. 2000.

[4] Sheikh, D. A.; Connell, S. J.; Dummer, R. S. "Durable silver coating for Kepler Space Telescope primary mirror." Proc. SPIE 7010, Space Telescopes and Instrumentation 2008: Optical, Infrared, and Millimeter, 70104E (July 12, 2008); doi:10.1117/12.789996, 2008.

[5] LaRue, R., private communication, 2020.

[6] Rodenburg, K., private communication, 2020.

[7] Custom Astronomy Filters, Custom Scientific https://customscientific.com/research_astronomy.html, 2020.

[8] Saadia, J. and Sheikh, D., MCAT 1.3 Measurement and Testing Results, ZeCoat Corporation, 2018.

[9] http://www2.oberlin.edu/physics/Scofield/p268/library/Ch-03%20Sunlight.pdf

[10] https://www.researchgate.net/publication/271891094_Design_and_Fabrication_of_an_Albedo_Insensitive_Analog_Sun_Sensor

[11] https://www.newport.com/t/introduction-to-solar-radiation

[12] This research has made use of the VizieR catalogue access tool, CDS, Strasbourg, France (DOI : 10.26093/cds/vizier). The original description of the VizieR service was published in 2000, A&AS 143, 23.

[13] Gaia Collaboration, *et al*., Gaia Data Release 2. Summary of the contents and survey properties, 2018 A&A, 616, 1

[14] Scott, David W. "On Optimal and Data-Based Histograms." *Biometrika*, vol. 66, no. 3, 1979, pp. 605–610., doi:10.1093/biomet/66.3.605.

[15] Abercromby, *et al*, Michigan Orbital DEbris Survey Telescope Observations of the Geosynchronous Orbital Debris Environment Observing Years: 2007–2009, NASA/TP-2011-217350.